2012 12th IEEE International Conference on Nanotechnology (IEEE-NANO)
The International Conference Centre Birmingham
20-23 August 20112, Birmingham, United Kingdom

Trapping and Patterning Nanoparticles from Spray

Marcel Tichem, Richard R. A. Syms, *Senior Member, IEEE*

***Abstract*— Gas-phase self-assembly of nanoparticles into microscale patterns by spray deposition and dielectrophoresis is demonstrated. Fluorescent nanospheres are sprayed using two different modes, pneumatic spray and electrospray. Nanospheres are trapped using microfabricated RF electrodes driven by both DC and AC voltages and the resulting particle distributions are visualised using confocal fluorescence microscopy. Pneumatic spray and dielectrophoresis leads to sharply defined patterns at electrode edges, at the expense of particle clustering. In contrast, nanospray dielectrophoresis leads to improved particle dispersion due to charge repulsion, but suffers from DC focusing effects due to surface charges. Controlled switching between the different modes is demonstrated, by manipulating the charge-state of the nanospheres and the trapping potential.**

I. Introduction

VOLUME production processes are required for the integration of nanoparticles such as carbon nanotubes (CNTs) and nanowires into materials and devices with novel properties and functions. In monolithic patterning approaches, the nanoparticles are grown or fabricated in-situ but this approach places significant demands on process compatibility. In heterogeneous integration, they are pre-fabricated and guided into the desired arrangement. This approach offers more freedom in processing, at the cost of increased patterning effort.

One possibility is self-assembly, based on field-driven alignment and trapping. Many physical forces have now been investigated, including viscous forces in gas flow [1] and in liquids [2, 3], optical trapping [4, 5] and magnetic fields [6]. In electrostatic patterning, charged objects are trapped by a DC potential [7-9]. In dielectrophoresis (DEP), dielectric particles form dipoles that are subject to a net force in an inhomogeneous electric field [10]. DEP has been explored quite extensively for nano-scale patterning, concentrating and sorting, using both DC and AC fields [11-17]. AC dielectrophoresis offers considerably more freedom than either Coulomb forces or DC dielectrophoresis. The force is in both sign and magnitude a function of the particle size and orientation, its dielectric properties, and the frequency and strength of the applied field, allowing considerable potential for separation and sorting.

In most of the examples above, the nanoparticles were held in suspension. Scavenging from the gas phase, generated by a spray system, has several advantages: a significant reduction in viscous force, and a consequent increase in trapping speed, the ability to direct the spray, and the yield of a dry product. Electrospray is a standard method of nanoparticle deposition [18, 19]. However, spray-based patterning has been largely ignored. Direct writing has been carried out by substrate translation [20], and stencil patterning has been achieved using apertures [21] and attractive DC forces [22].

Here we investigate gas-phase trapping. We compare different combinations of pneumatic and electrospray with dielectrophoresis for the patterned deposition of fluorescent nanospheres, and evaluate the effect of DC charge. We show that there is competition between the effects of viscous drag, Coulomb force, and both DC and AC dielectrophoretic forces. Section II introduces the concepts involved, and Section III presents a theoretical model of the most successful trap type investigated, a microfabricated microstrip. Section IV describes the experimental method and result and demonstrates controlled manipulation of the trapping mode. Section V presents conclusions.

II. Spraying and Trapping Modes

We have explored two methods for spray generation: pneumatic spray and electrospray. In pneumatic spray, droplets formed at the end of a narrow capillary are atomised by a coaxial gas flow. The gas promotes solvent evaporation, leaving suspended nanoparticles to be transported by viscous drag, together with residual solvent droplets. The spray humidity is a function of the distance from the spray origin, and can be reduced by heating the gas. Since the particles are uncharged, they will be forced together by surface tension during evaporation. Large dielectric clusters may easily be trapped using both DC and AC DEP forces.

In electrospray, a co-axial nebuliser is again used. However, the spray is primarily generated using a DC field from a voltage V_D (typically, several kV) applied between the solution and a nearby electrode. Three phases can be distinguished: formation of a Taylor cone from the meniscus at the capillary tip, extrusion of a jet, and separation of the jet into a plume due to Coulomb repulsion. Solvent evaporation again takes place in the plume, leaving a mixture of ions in the flow. In nanospray, a small-diameter (10-50 μm ID) capillary is used to reduce the extraction voltage to around 1 kV, without a significant reduction in the

Manuscript received June 20, 2012. This work was supported by the EU FP7 Marie Curie IEF grant 253731 "Discrete Volume Assembly at Nano-scale (DIVAN)".

M. Tichem was with the Optical and Semiconductor Devices Group, Department of Electrical and Electronic Engineering, Imperial College, Exhibition Road, London SW7 2BT, U.K, on leave from the Micro and Nano Engineering Laboratory, Delft University of Technology, Mekelweg 2, 2628CD, Delft, The Netherlands (phone: +31 15 2781603; e-mail: m.tichem@tudelft.nl).

R.R.A. Syms is with the Optical and Semiconductor Devices Group, Department of Electrical and Electronic Engineering, Imperial College, Exhibition Road, London SW7 2BT, U.K (e-mail: r.syms@ic.ac.uk).

ion density [23]. Nanoparticles may also be carried in the spray. Since they are now charged, electrostatic repulsion allows a much finer dispersion, but leads to other effects that complicate trapping.

Trapping is achieved by placing electrodes provided with appropriate AC and DC potentials in the spray path. Fig. 1 shows example geometries, together with sketches of their equipotentials on a 2D plane. The simplest is a pair of coplanar electrodes on an insulating layer as shown in Fig. 1a. In this case, the electric field forms two concentrations, one at each electrode tip, which provides two DEP trapping foci. Fig. 1b shows an alternative arrangement consisting of a conducting strip above a ground plane. For a dielectric interlayer with a relative permittivity close to unity, this arrangement is equivalent to a conducting strip spaced at approximately twice the distance from a second virtual strip electrode. In this case, four DEP foci are formed, one at each electrode edge; however, only the real foci are important. This configuration has the advantage of reduced sensitivity to dielectric breakdown, especially in a humid spray. Consequently, much of the remainder of the paper is focused on this geometry. However, exposed dielectric may alter behaviour if the nanospheres are charged.

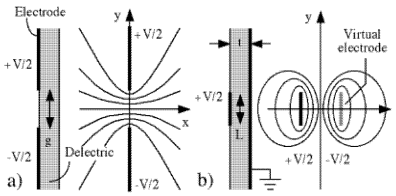

Fig. 1. Geometries for microfabricated traps and sketches of their associated equipotentials: a) coplanar, and b) microstrip.

Each configuration may be used with either pneumatic or electrospray sources, with an AC potential applied using a signal generator via a step-up transformer. However, for electrospray, DC potentials must also be controlled. Fig. 2 shows an example arrangement for a microstrip trap, in which voltages V_{D1} and V_{D2} are used to generate the spray and apply a bias to the trap, respectively. The voltage dropped across resistors R_E and R_C can be used to monitor ion emission and ion collection.

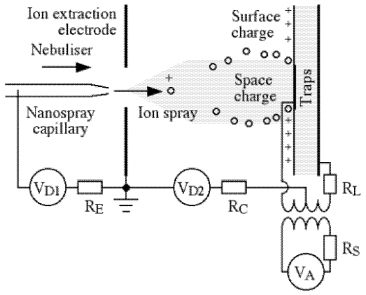

Fig. 2. Arrangement for nanospray-dielectrophoresis.

III. THEORETICAL MODEL

Dielectrophoretic scavenging of neutral particles from a gas flow involves a combination of physical effects: inertial and gravitational forces, drag forces due to the gas, and DEP forces in the trapping area. Inertial and gravitational forces can be ignored at the nano size scale. The drag force is responsible for transportation, and the particles will typically be carried towards and along the trapping surface. When particles are sufficiently close to a trap and moving slowly enough, they will be guided towards it by the dielectrophoretic force, which may be both DC or AC. Closely separated particles that are uncharged but polarised may also form pearl chains.

In nanospray-dielectrophoresis, there will be additional Coulomb forces. For example, there will be a space charge within the plume, which may prevent chain formation. The charges of any ions landing on the trapping electrodes will be conducted away. However, microfabricated traps will typically be fabricated on a dielectric, which will charge and then generate a repulsive force for subsequent ions. Surface charging will therefore continue only until equilibrium preventing further accumulation is achieved. Non-uniform flux will then give rise to DC dielectrophoresis even if no DC voltage is present. Finally, if charged particles are sufficiently close to a substrate, image fields will be generated, resulting in additional attractive forces. However, these are short-range.

We have developed an independent-particle model, in which trajectories are determined by solving Newton‟s equation for drag, DEP and electrostatic forces. The first can be determined using the flow of an ideal fluid, while the second and third can be found by solving the Laplace equation, with fixed electrode potentials. Equilibrium surface charges are also described by fixed potentials. Complexity is further reduced by restriction to two dimensions. In this simplified approach, the equation of motion for an independent particle (assumed spherical) is:

$$\underline{F}_D + \underline{F}_S + \underline{F}_{DC} + \underline{F}_{AC} = 0 \quad (1)$$

Here $\underline{F}_D$ is the viscous drag force given by Stokes‟ law:

$$\underline{F}_D = -6\pi\eta R(\underline{u} - \underline{u}_M) \quad (2)$$

Here $\underline{u}$ is the particle velocity, $\underline{u}_M$ is the velocity of the background medium, R is the particle radius and η is the viscosity. The background flow may be modelled by assuming that the gas is an ideal fluid. In this case, for a flow impinging from the -ve x direction, the velocity distribution $\underline{u}_M$ on the (x, y) plane can be determined from the stream function ψ_M, using the relations $u_{Mx} = -\partial\psi_M/\partial y$ and $u_{My} = \partial\psi_M/\partial x$. For irrotational flow, the stream function satisfies Laplace‟s equation $\nabla^2\psi_M = 0$ and contours of constant ψ_M are streamlines. For a flow impinging normally on a plate perpendicular to the x-axis, the boundary conditions are $u_{Mx} = 0$ on $x = 0$ (the plate), and $u_{My} = 0$ for large, negative x and small y. A suitable stream function is $\psi_M = Axy$, where A is a constant, giving $u_{Mx} = -Ax$ and $u_{My} = +Ay$.

Similarly, $\underline{F}_S$ is the electrostatic force, given by:

$$\underline{F}_S = q\underline{E}_S \quad (3)$$

Here $\underline{E}_S$ is the static electric field and q is the charge on the particle. The static field is determined as $\underline{E} = -\nabla\phi_S$, where ϕ_S is the solution of Laplace"s equation $\nabla^2\phi_S = 0$ for a system of fixed electrode potentials. For thick electrodes and dielectric substrates, Laplace"s equation must generally be solved numerically (for example, by over-relaxation).

The DEP force has two components, a DC component $\underline{F}_{DC}$ resulting from any time-independent field non-uniformity and an AC component $\underline{F}_{AC}$ resulting from time-varying inhomogeneous fields. Both components can be described by the same expression (again, for a spherical particle):

$$\underline{F} = 2\pi R^3 \varepsilon_M \, \mathrm{Re}[f_{CM}(\omega)] \, \nabla |\underline{E}|^2 \tag{4}$$

Here $\underline{E}$ is the electric field, taken as either $\underline{E}_S$ (for static fields) or $\underline{E}_{rms}$ (for AC fields). Similarly, $f_{CM}(\omega)$ is the Clausius-Mosotti factor, to be evaluated at DC for a static field and a specific angular frequency ω for an AC field, and is given by:

$$f_{CM} = (\varepsilon_S - \varepsilon_M) / (\varepsilon_S + 2\varepsilon_M) \tag{5}$$

Here ε_S and ε_M are the complex dielectric constants of the sphere and the surrounding medium respectively. In the quasi-static approximation, the field $\underline{E}_{rms}$ may again be determined by solving Laplace"s equation numerically for a different set of surface potentials representing the AC electric field amplitudes. Combination of Equations 1-5 then leads to the trajectory equation:

$$\underline{u} = \underline{u}_M + k_S \underline{E}_S + k_{DC} \nabla |\underline{E}_S|^2 + k_{AC} \nabla |\underline{E}_{rms}|^2 \tag{6}$$

Here the coefficients k_S, k_{DC} and k_{AC} are given by:

$$\begin{aligned} k_S &= q/6\pi\eta R \\ k_{DC} &= (R^2\varepsilon_M/3\eta) \, \mathrm{Re}[f_{CM}(0)] \\ k_{AC} &= (R^2\varepsilon_M/3\eta) \, \mathrm{Re}[f_{CM}(\omega)] \end{aligned} \tag{7}$$

The presence of η in the denominator of all coefficients implies that trapping from a gas is likely to be much faster than from a liquid, although the resulting trajectories are likely to be similar. Since $\underline{u} = d\underline{r}/dt$, where $\underline{r}$ is the position vector and t is time, we may then obtain:

$$\begin{aligned} dx/dt &= u_{Mx} + k_S \underline{E}_{Sx} + k_{DC} \partial |\underline{E}_S|^2/\partial x + k_{AC} \partial |\underline{E}_{rms}|^2/\partial x \\ dy/dt &= u_{My} + k_S \underline{E}_{Sy} + k_{DC} \partial |\underline{E}_S|^2/\partial y + k_{AC} \partial |\underline{E}_{rms}|^2/\partial y \\ dy/dx &= u_y/u_x \end{aligned} \tag{8}$$

Equations 8 may then be integrated numerically from given starting conditions. Clearly, if there are no fields, $dy/dx = u_{My}/u_{Mx}$ and the trajectories follow the gas streamlines. Fields then modify the trajectories. The result will depend strongly on the exact system parameters. In detail these include nanoparticle properties (dielectric constant, radius, charge), gas properties (viscosity, dielectric constant) and operational parameters (gas flow velocity, electric field definition). More generally the relative significance of different effects depends mainly on the field and coefficient magnitudes. The various regimes may therefore be illustrated by assuming electrode potentials as either ±1V as required and varying the k-values.

Fig. 3 shows results of numerical solutions to Equations 8. We assumed a microstrip trap of width 10 µm separated from a ground plane by a 20 µm thick air-gap, and that electric fields are derived from voltages of plus or minus unity for both DC and AC potentials. Results are plotted over a range from -50 µm to +50 µm around the trap.

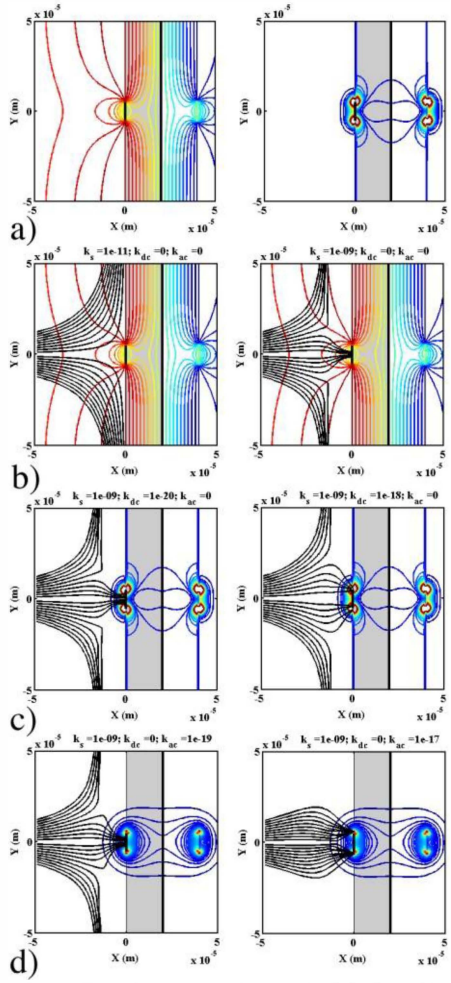

Fig. 3. a) Equipotentials (LH) and trapping potentials (RH) for DC fields; and trajectories during DC charge repulsion, for increasing values of b) k_S; c) k_{DC} and d) k_{AC}.

Fig. 3a shows the equipotentials (LH) and normalised trapping potential (RH) due to uniform DC charging of areas outside the electrode surface, assuming the electrodes themselves are grounded. These are derived from the real potentials and a set of „image" potentials. The trapping potential has four foci, two real and two virtual. Fig. 3b shows particle trajectories for different values of k_S, increasing over two orders of magnitude, superimposed on the DC equipotentials. For small k_S, the flow stream approaches the trapping plane and then diverges. However as k_{DC} rises, two effects can be seen. Off-axis trajectories are

repelled from the DC potential barrier created by the charged surfaces, while on-axis trajectories are forced towards the centre of the trapping electrode. The first phenomenon should result in a reduction in random surface decoration, while the second phenomenon leads to charge heaping. Similar effects are observed when the strip electrode is held at an attractive potential designed to mimic DC trapping.

Fig. 3c show similar trajectories for a fixed value of k_S but different values of k_{DC}, superimposed on contours of normalised DC trapping potential. For small k_{DC}, charge repulsion and heaping occur as before. However, as k_{DC} rises, nanoparticles previously forced towards the electrode centre are now trapped by DC dielectrophoresis at the electrode edge. However, since k_{DC} is strictly proportional to k_S, we might expect the effect to be small. Conversely, since k_{AC} is an independent variable, we might expect much larger AC trapping effects. Fig. 3d shows similar trajectories for a fixed value of k_S but different values of k_{AC}, now superimposed on contours of normalised AC trapping potential. For small k_{AC}, charge repulsion and charge heaping occur as before. However, as k_{AC} rises, nanoparticles are increasingly trapped by AC dielectrophoresis. This result shows that AC trapping can also ovecome the joint effects of charge repulsion and charge heaping when the voltage is large enough.

We may summarize these results as follows. Trapping is determined from a balance of the forces involved. For neutral particles, particles are either trapped or not, depending on the gas flow rate and the starting condition. Particles starting strongly off-axis in a relatively strong gas flow are not trapped, and trapping probability is increased towards the centre of weaker flows. The trajectories of trapped particles end at electrode edges where the trapping foci are located. However, for charged particles, some trajectories are forced away from these foci towards the electrode centres, due to surface charge repulsion.

IV. Experimental Results

A Perspex experimental rig was developed that allows fluorescent nanoparticles to be sprayed perpendicularly onto a microfabricated chip carrying patterned electrodes as shown in Fig. 4. The set-up allows both pneumatic spray and nanospray. Liquid flow was generated using a programmable syringe pump (KD Scientific 100 series) with a glass syringe (Hamilton 250 µL), which continuously delivers spray solution at low flow rates to a nanospray capillary (New Objective SilicaTips™, proximal metal coating, 30 µm ID). A 1 mm ID co-axial nebulizer was used to provide a continuous flow of N_2 from a gas cylinder. The gas was heated using an electrical heater leading to nebulizer gas temperatures of ≈ 30 °C.

For electrospray, a thin photoetched stainless steel electrode with a circular aperture (800 µm diameter) was placed at a short distance (100 - 150 µm) from the capillary tip. A high voltage DC power supply (HP 6515A) generated the voltage between the tip and the counter-electrode, and a low-voltage PSU was used to control the DC potential of the trap. An electrometer (Keithley 6517) was used to monitor the spray, by measuring the voltage across a current-limiting resistor. The DC voltage was in 1.0 - 1.4 kV, the solution was supplied with a flow rate of 12 - 15 µL/hr, and the nebuliser gas flow rate was tuned to achieve a stable spray. The trapping electrodes were at a distance of 1 - 1.5 cm, and spraying was carried out for 2-4 minutes. For pneumatic spraying, the counter-electrode and the DC power supplies and monitors were simply removed, so that an aerosol was generated directly. Larger gas flow rates were required to achieve atomization, and the trapping electrodes could then be placed at a larger distance (2 - 4 cm) from the capillary.

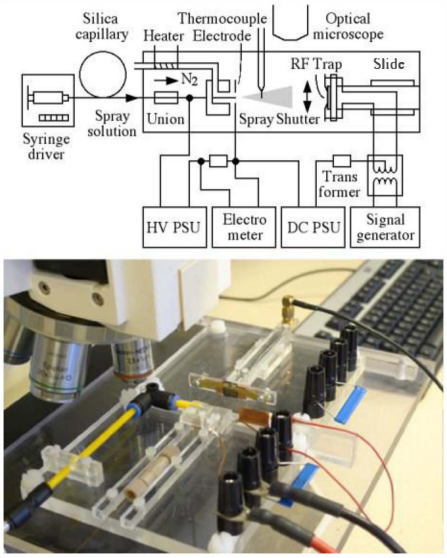

Fig. 4. Arrangement and realisation of experimental rig.

The trapping system was a chip with different planar electrode configurations, as shown in Fig. 5. The fingers were connected to bus bars to connect all electrode pairs to the drive voltage. The fingers and bus bars are 20 µm and 50 µm wide, respectively, and the electrode gaps are 20 µm. The chip was fabricated on a <100> Si wafer, with a 20 µm thick SiO_2 insulation layer and Cr/Au electrodes.

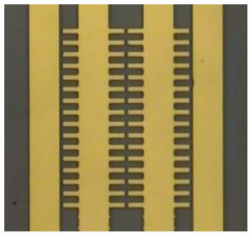

Fig. 5. Detail of the trapping electrodes.

DC voltages were generated using a low voltage PSU, and AC voltages using a signal generator (Thandar TG1010) and a step-up transformer, reaching maximum voltages of 300 V p-p at 10 kHz. In-plane traps were realised by connecting to opposing electrode sets. Microstrip traps were realised by connecting all surface electrodes to a common potential and connecting with silver-loaded epoxy to the Si substrate, which then provided a ground plane. However, some distortion of the AC signal was observed in this mode, presumably due to diode behaviour at the silicon contact.

The nanoparticles were 50 nm diameter fluorescent spheres (Sigma Aldrich L0780, amine-modified polystyrene) with excitation and emission wavelengths of λ_{ex} ~360 nm and λ_{em} ~420 nm, respectively. The nanospheres were dispersed in a solvent consisting of 75% DI water, 20% methanol and 5% acetic acid to increase the conductivity. Solution preparation involved addition of a small additional amount (< 1%) of surfactant and sonication for at least 15 minutes. Cone-jet formation was observed using an optical microscope, and stable spraying was achieved at 0.05 - 0.1 vol. % concentration of nanospheres, as shown in Fig. 6.

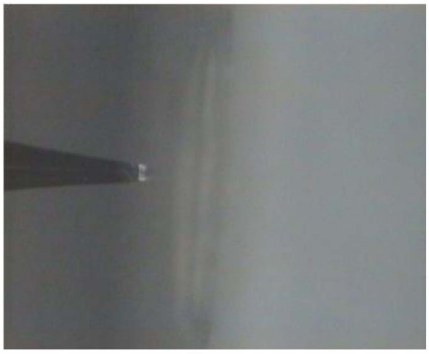

Fig. 6. Nanospray capillary tip during electrospray.

Examination of the deposited patterns was carried out with a confocal fluorescence microscope (Leica SP5) equipped with an Ar^+ laser for visible imaging and a tuneable multi-photon laser (Spectra-Physics Mai Tai® Ti:sapphire) for fluorescence imaging, as shown in Fig. 7. The combination allows optical images of the electrode system and the fluorescent nanosphere patterns to be acquired separately and subsequently overlaid.

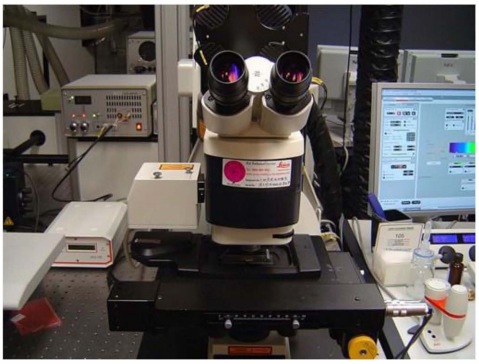

Fig. 7. Confocal fluorescence microscope.

Several different experiments were carried out. Both pneumatic and electrospraying modes were used, DC and AC voltages were applied to the electrodes, and in-plane and microstrip electrodes were investigated. In-plane electrodes were generally damaged by a plasma discharge, as shown in Fig. 8. Microstrip electrodes routinely gave more successful results, especially with careful dehydration of the spray.

Fig. 9a shows a uniform surface decoration obtained while pneumatically spraying onto a microstrip trap without an applied voltage. This figure demonstrates the relatively uniform coating obtained without a trapping field. Fig. 9b shows the corresponding pattern obtained during electrospray with a simple DC attractive potential. Here the decoration approximately follows the electrode shapes, but charge heaping has forced the nanospheres to lie within the electrode areas. There is little edge decoration, suggesting that DC dielectrophoretic effects are indeed relatively unimportant. A subsidiary effect of surface charging is to reduce contamination of the dielectric areas.

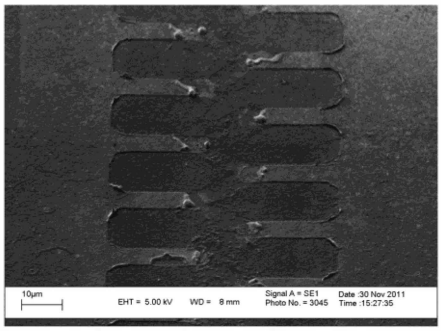

Fig. 8. SEM photo of plasma discharge effects with in-plane electrodes.

Fig. 9c shows the corresponding result obtained during electrospray with an AC trapping voltage. The results are generally similar to Fig. 9b. However, an additional edge decoration has clearly been induced by AC dielectrophoresis, and a thin nanosphere pattern can now be seen, following the electrode outline. Finally, Fig. 9d shows the result achieved during pneumatic spray with an AC voltage applied. Trapping is now achieved without any charge heaping; only the electrode outline may be seen, and the main electrode areas are no longer coated. However, a uniform, random distribution of deposit is visible elsewhere. These results confirm the predictions of the analytic model, and demonstrate that switching between the different trapping modes may be achieved using careful control of the nanosphere charge-state and the trapping potential.

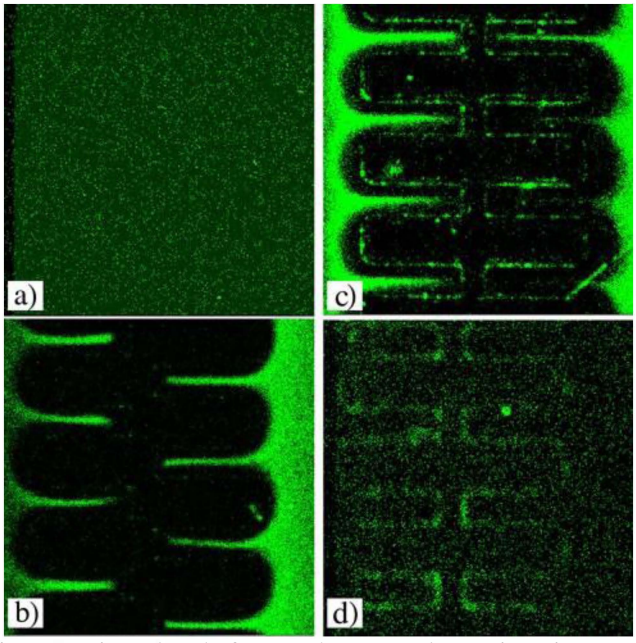

Fig. 9. Experimental results for nanospheres sprayed onto microstrip traps; a) pneumatic spray, no applied voltage; b) electrospray with DC voltage; c) electrospray with AC voltage; d) pneumatic spray with AC voltage.

V. CONCLUSIONS

We have demonstrated trapping of nanoparticles from spray, using different combinations of pneumatic spray, electrospray and DC and AC trapping forces. Scavenging particles from a gas rather than a liquid phase has the advantage of reduced viscous forces, so that rapid coating may be achieved, the spray may be directed towards the trapping region, and the deposit is inherently dry. All aspects offer improvements in trapping performance.

Experimental results confirm an independent-particle model that includes the effect of viscous drag, DC and AC potentials, and their spatial variations. Both show that different patterning effects can be achieved using combinations of spraying modes and trapping fields. Trapping can be carried out from pneumatically generated spray and electrospray. The former has the potential for cleaner patterns, since it forms a deposit mainly in designated trapping regions. However, the latter is likely to generate a more uniform dispersion. DC fields can also trap charged nanoparticles. In this case, patterns generally follow the electrode shapes, but repulsive forces from adjacent surface charges lead to patterns smaller than electrode dimensions. AC dielectrophoresis can trap both charged and uncharged nanoparticles, and has the potential for higher resolution since the deposits follow electrode edges.

ACKNOWLEDGEMENT

The authors are extremely grateful to Mr. Phil Jones for fabrication of the experimental set-up, to Dr. Kaushal Choonee for fabrication of the microelectrode array and to Dr. Martin Spitaler for support in fluorescence imaging.

REFERENCES

[1] Xin, H., A.T. Woolley (2004). "Directional orientation of carbon nanotubes on surfaces using a gas flow cell" Nano Letts. **4**: 1481-1484.

[2] Kralchevsky, P.A., N.D. Denkov et al. (1994). "Formation of 2-dimensional colloid crystals in liquid-films under the action of capillary forces" J. Phys. Cond. Matt **6**, A395-A402.

[3] Liddle, J.A., Y. Cui, et al. (2004). "Lithographically directed self-assembly of nanostructures" J. Vac. Sci. Technol. B **22**: 3409-3414.

[4] Tan, S., H.A. Lopez et al. (2004). "Optical trapping of single-walled carbon nanotubes" Nano Letts. **4**: 1415-1419.

[5] Yu, T., Cheung F.-C., Sow C.-H. "The manipulation and assembly of CuO nanorods with line optical tweezers" Nanotechnology 15, 1732-1736 (2004).

[6] Tanase, M., D.M. Silevitch et al. (2002). "Magnetic trapping and self-assembly of multicomponent nanowires" J. Appl. Phys. **91**: 8459-8551.

[7] Naujoks, N. and A. Stemmer (2005). "Micro- and nanoxerography in liquids – controlling pattern definition" Microelectr. Eng. **78-79**: 331–337.

[8] Mesquida, P., A. Stemmer (2002). "Maskless nanofabrication using the electrostatic attachment of gold particles to electrically patterned surfaces" Microelectr. Engng. **61-62**: 671-674.

[9] Jacobs, H.O., S.A. Campbell, et al. (2002). "Approaching nanoxerography: the use of electrostatic forces to position nanoparticles with 100 nm scale resolution" Adv. Mats. **14**: 1553-1557.

[10] Pohl, H.A. (1978). *"Dielectrophoresis"*, Cambridge University Press, Cambridge.

[11] Smith, P.A., C.D. Nordquist, et al. (2000). "Electric-field assisted assembly and alignment of metallic nanowires." Appl. Phys. Letts. **77**: 1399-1401.

[12] Hermanson, K.D., S.O. Lumsdon et al. (2001). "Dielectrophoretic assembly of electrically functional microwires from nanoparticle suspensions" Science **294**: 1082-1086.

[13] Krupke, R., F. Hennrich, et al. (2004). "Surface conductance induced dielectrophoresis of semiconducting single-walled carbon nanotubes" Nano Letts. **4**: 1395-1399.

[14] Cummings, E.B. and A.K. Singh (2003). "Dielectrophoresis in microchips containing arrays of insulating posts: theoretical and experimental results" Anal Chem **75**: 4724-4731.

[15] Chen, D.C., H. Du, et al. (2010). "Rapid concentration of nanoparticles with DC dielectrophoresis in focused electric fields." Nanoscale Res. Letts. **5**: 55-60.

[16] Green, N.G., Morgan H. (1997) "Dielectrophoretic separation of nanoparticles" J. Phys. D. Appl. Phys. **30**: L41-L84.

[17] Zhang, C., K. Khooshmanesh et al. (2009). "Dielectrophoretic separation of carbon nanotubes and polystyrene microparticles" Microfluid. Nanofluid. **7**: 633-645.

[18] Salata, OV. (2005) "Tools of nanotechnology: electrospray" Curr. Nanosci. **1**: 25-33.

[19] Jaworek, A., A.T. Sobczyk (2008). "Electrospraying route to nanotechnology: an overview" J. Electrostat. **66**: 197-219.

[20] Khan, S., Y.H. Doh (2011). "Direct patterning and electrospray deposition through EHD for fabrication of printed thin film transistors" Curr. Appl. Phys. **11**: S217-S279.

[21] Kim, J.-W., Y. Yamagata, et al. (2009). "Direct and dry micro-patterning of nano-particles by electrospray deposition through a micro-stencil mask" J. Micromech. Microeng. **19**: 025021.

[22] Welle, A.M., H.O. Jacobs (2005). "Printing of organic and inorganic nanomaterials using electrospray ionization and Coulomb-force directed assembly" Appl. Phys. Lett. **87**: 263119.

[23] Gale, D.C., Smith R.D. (1993) "Small volume and low flow-rate electrospray ionization mass spectrometry of aqueous samples" Rapid Comm. in Mass Spectrom. **7**, 1017-1021.

Marcel Tichem is an Associate Professor at the Micro and Nano Engineering Laboratory, Faculty of Mechanical, Maritime and Materials Engineering, Delft University of Technology. His research program focuses on micro and nano assembly. Specific research interests include photonic integration and sub-micrometer alignment using passive and active microfabricated structures, self-assembly at micro-scale, foil-based systems, and nano-scale patterning. He coordinates the EU FP7 funded collaborative project Chip2Foil. During 2011 he worked at the Optical and Semiconductor Devices Group in the EEE Dept, Imperial College London, on the basis of an EU FP7 Marie Curie IEF training grant to explore volume manufacturing methods for realising discrete patterns of nano-scale objects.

Richard R.A. Syms has been Professor of Microsystems Technology in the EEE Dept, Imperial College London, since 1996. He currently lectures on guided wave optics and electromagnetic theory. He has published over 150 journal papers, 80 conference papers and two books on holography, integrated optics, metamaterials and microengineering. Most recently he has been developing 3D self-assembling micro-structures. miniature quadrupole mass spectrometers, optical MEMS such variable attenuators and tunable lasers, and RF probes for magnetic resonance imaging, He has consulted widely on guided wave optics and MEMS, and co-founded the MEMS spin-out company Microsaic Systems in 2001. He currently acts as an Associate Editor for JMEMS and for Metamaterials. He has served on many MEMS review panels, including for the EPSRC Microsystems Technology Integration Program, and the German, Canadian and Singaporean MEMS programs. He is a Fellow of the Royal Academy of Engineering, the Institute of Physics and the Institute of Electrical Engineers.